Concentrations of Gd-BOPTA in cholestatic fatty rat livers: role of transport functions through membrane proteins

Pastor, Catherine; Wissmeyer, Michael; Millet, Philippe

CONTRAST MEDIA & MOLECULAR IMAGING

Received: 19 June 2012, Revised: 30 August 2012, Accepted: 15 September 2012, Published online in Wiley Online Library: 2012

(wileyonlinelibrary.com) DOI: 10.1002/cmmi.1511

Concentrations of Gd–BOPTA in cholestatic fatty rat livers: role of transport functions through membrane proteins

Catherine M. Pastor[a]*, Michael Wissmeyer[b] and Philippe Millet[c]

Gd–BOPTA (gadobenate dimeglumine) is a magnetic resonance (MR) contrast agent that, after i.v. administration, distributes within the extracellular space, enters rat hepatocytes through the sinusoidal transporters organic anion transporting peptides (Oatps) and is excreted unchanged into bile through the multidrug resistance-associated protein 2 (Mrp2). It is unclear how the hepatobiliary contrast agent would accumulate in cholestatic fatty livers from obese rats with bile flow impairment. Indeed, the expression of both Oatps and Mrp2 transporters is decreased in cholestatic hepatocytes. To assess this question, we measured on-line the hepatic concentrations of ^{153}Gd–BOPTA with a gamma probe placed over perfused rat livers. During the perfusion of ^{153}Gd–BOPTA, we obtained a similar maximal hepatic concentration in normal and fatty livers despite the decreased expression and function of membrane transporters in fatty livers. By pharmacokinetic modeling and mathematical simulations, we show how changes of transport into and out of hepatocytes modify the concentrations of ^{153}Gd–BOPTA within hepatocytes. Mathematical simulations help to understand how each parameter (entry into hepatocytes, bile excretion, or efflux back to sinusoids) interferes with the hepatic concentrations. The hepatic concentrations of ^{153}Gd–BOPTA within hepatocytes rely on the entry into hepatocytes through the sinusoidal membrane and on two paths of exit, the efflux back to sinusoids and the elimination into bile. Understanding how ^{153}Gd–BOPTA accumulates in hepatocytes is then complex. However, such understanding is important to analyze liver imaging with hepatobiliary contrast agents in cholestatic fatty livers.

Keywords: MR hepatobiliary contrast agent; liver MRI; cellular transport

1. INTRODUCTION

Nonalcoholic fatty liver diseases include a large spectrum of abnormalities characterized by an increased intrahepatic triglyceride content (steatosis) with or without inflammation and fibrosis (1). The transition from fatty livers to more severe disease (or steatohepatitis) is triggered by inflammation. Cholestasis (or decreased bile flow) is an important marker of this increased severity. Cholestasis is associated with the dysregulation of proteins involved in the transport of bile acids, phospholipids, sterols and organic anions through hepatocytes (2–5). Interestingly, when the bile excretion of xenobiotics and endobiotics or their metabolites is impaired, the upregulation of transporters located in the sinusoidal membrane may favor their efflux back into sinusoidal blood, preventing a potentially harmful accumulation within hepatocytes (6). The expression of hepatic transporters during cholestasis is modified, but the consequences on the hepatic accumulation of hepatobiliary compounds are largely unknown. Interestingly, various liver imaging techniques have been developed to assess fatty livers in patients (7–9). Few experimental and clinical studies have used magnetic resonance imaging (MRI) with hepatobiliary contrast agents to characterize these livers (10–12).

We previously showed that hepatic concentrations of ^{153}Gd–BOPTA can be measured on-line using a gamma scintillation probe placed over rat livers (13). Gd–BOPTA, the active moiety of gadobenate dimeglumine (MultiHance®, Bracco Milan), is an MR contrast agent that distributes within the extracellular hepatic space and enters into hepatocytes through the sinusoidal transporters organic anion transporting peptides (Oatp1a1, Oatp1a4, and Oatp1b2) (14). Gd–BOPTA is not metabolized during its transport to the canalicular membrane and is excreted unchanged into bile through Mrp2 (14,15). At liver MRI, Gd–BOPTA remains within the extracellular space in rat livers with severe cirrhosis that lack sinusoidal transporters (16).

Because cholestatic fatty livers have a decreased expression of Oatp1a4 (17,18) and Mrp2 (17,19), we hypothesized that Gd–BOPTA would differently accumulate within cholestatic hepatocytes. Moreover, cholestasis may also modify the transport of Gd–BOPTA through the transporters. The aim of the present study was then to compare the pharmacokinetics of Gd–BOPTA concentrations in normal and cholestatic rat fatty livers and to

* *Correspondence to: C. M. Pastor, Laboratoire de Physiopathologie Hépatique et Imagerie Moléculaire Hôpitaux Universitaires de Genève, Geneva, Switzerland. Email: catherine.pastor@hcuge.ch*

a *C. M. Pastor*
Laboratoire de Physiopathologie Hépatique et Imagerie Moléculaire

b *M. Wissmeyer*
Service de Médecine Nucléaire

c *P. Millet*
Unité de Neurophysiologie Clinique et Neuroimagerie Hôpitaux Universitaires de Genève, Geneva, Switzerland

understand how the transport through cell membrane proteins generates the concentrations within cholestatic hepatocytes.

2. MATERIALS AND METHODS

2.1. Animals

Before liver isolation, Zucker fat (*fa/fa*) and Zucker lean (*fa/+*) rats were anesthetized with pentobarbital (50 mg kg^{-1} i.p.). The protocol was approved by the animal welfare committee of the University of Geneva and the veterinary office and followed the guidelines for the care and use of laboratory animals.

2.2. Perfusion of Isolated Rat Livers

Livers were isolated and perfused *in situ* with a Krebs–Henseleit-bicarbonate (KHB) solution ± contrast agents using a nonrecirculating system (Fig. 1) (13). In each experiment, the flow rate was 30 ml min^{-1} and the bile duct was cannulated for bile sampling collection.

2.3. Quantification of Hepatic Concentrations

Gd–BOPTA was prepared by adding $^{153}GdCl_3$ to a 0.5 M Gd–BOPTA solution (1 MBq ml^{-1}), which contained a slight excess of the ligand BOPTA (20,21). To assess the hepatic concentrations induced by the perfusion of the extracellular contrast agent Gd–DTPA (gadopentetate dimeglumine, Magnevist®, Bayer, Zürich), Gd–DTPA was also prepared by adding $^{153}GdCl_3$ to a 0.5 M solution of Magnevist®. Gd–DTPA is an extracellular contrast agent, which has the same extracellular distribution as Gd–BOPTA but does not enter into hepatocytes (13,14). Both contrast agents were then diluted in KHB solution to obtain a 200 μM concentration to be perfused in rat livers.

To quantify the on-line hepatic concentrations of ^{153}Gd-labeled contrast agents, a gamma-scintillation probe that measures radioactivity every 20 s was placed 1 cm above the liver (Fig. 1A) (21). To transform radioactivity count rates into contrast agent amounts, the radioactivity in the entire liver at the end of each experiment was measured (Activimeter Isomed 2000, MCD

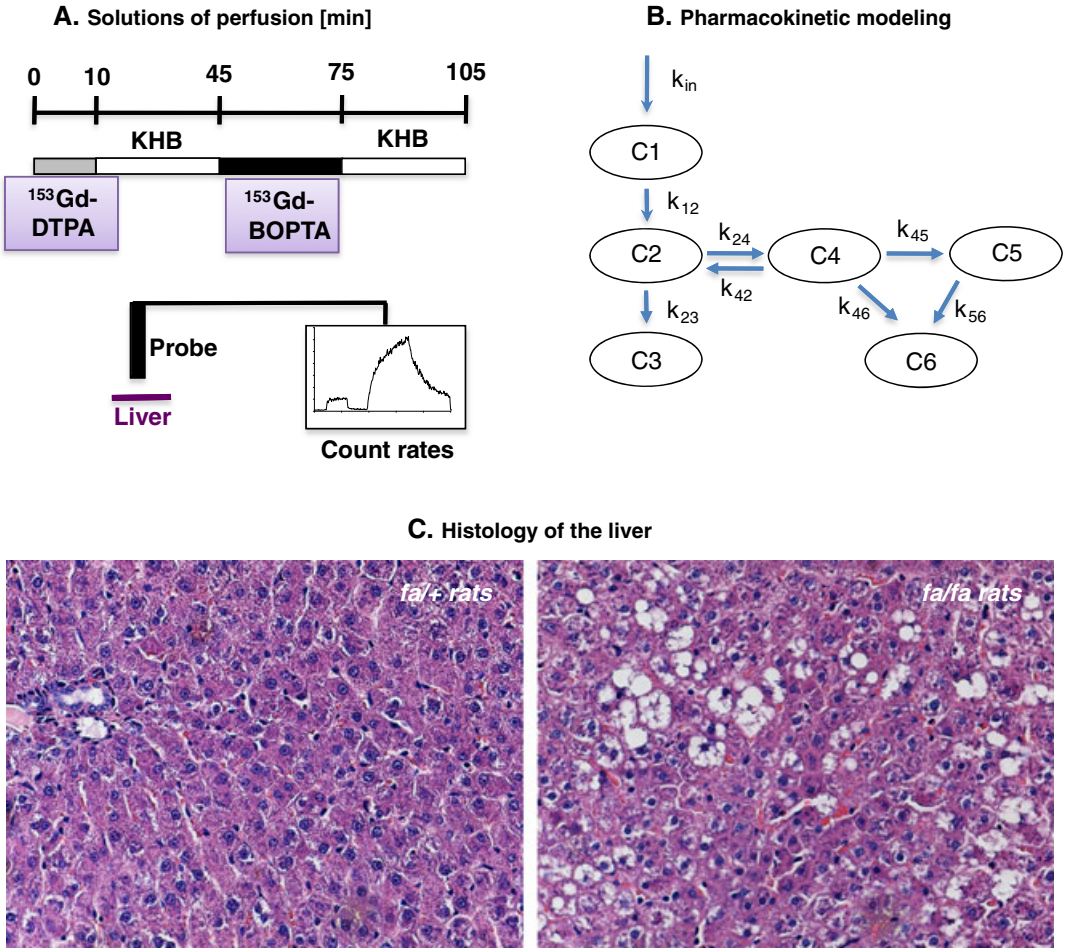

Figure 1. (A) Experimental protocol and data obtained during liver perfusion with the contrast agents ^{153}Gd–DTPA (200 μM during 10 min) and ^{153}Gd–BOPTA (200 μM during 30 min). The flow rate being 30 ml min^{-1}, the amount of ^{153}Gd–DTPA perfused was 60 μmol and that of ^{153}Gd–BOPTA was 180 μmol. To quantify the on-line hepatic concentrations of ^{153}Gd–labeled contrast agents, a gamma-scintillation probe that measures radioactivity every 20 s was placed above the liver. KHB, Krebs–Henseleit-bicarbonate solution. (B) Pharmacokinetic modeling of ^{153}Gd-BOPTA transport in rat perfused livers. Entry of contrast agent into the liver is modeled as a zero-order infusion rate K_{in}. Compartment C1 illustrates the dilution of ^{153}Gd–BOPTA at the beginning and at the end of perfusion. C2 is the extracellular space, C4 and C5 are two hepatocyte-associated spaces. C3 represents the amount of contrast agent in perfusate, and C6 in bile. First-order rate constants k_{ij} are defined with respect to *i*, the compartment of origin, and *j*, compartment of convergence. (C) Histology of the liver from obese (*fa/fa*) and normal (*fa/+*) rats is illustrated.

Nuklear Medizintechnik, Germany) and related to the last count rates measured by the probe.

2.4. Experimental Protocol

We perfused five livers isolated from *fa*/+ (control Zucker) rats and five livers isolated from *fa*/*fa* (fat Zucker) rats with KHB solution (15 min, recovery period), ^{153}Gd–DTPA (10 min), KHB solution (rinse period, 30 min), ^{153}Gd–BOPTA (30 min) and KHB solution (rinse period, 30 min; Fig. 1). Both contrast agents were perfused with a 200 μM concentrations. During each perfusion, we measured ^{153}Gd–BOPTA bile concentration (nmol g^{-1}), ^{153}Gd–BOPTA bile excretion rate (nmol min^{-1} g^{-1}), ^{153}Gd–BOPTA concentration within the liver (nmol g^{-1}) and bile flow (μl min^{-1} g^{-1}).

2.5. Liver Tests and Histology

Alanine amino transferases, cholesterol and triglycerides in serum were determined using a serum multiple analyzer. Liver tissue was fixed, embedded in paraffin (4 μM thick sections), and analyzed under light microscopy after hematoxylin and eosin staining.

2.6. Simulations in the Pharmacokinetic Model

In perfused livers isolated from control *fa*/+ rats, the compartment model that best described the amounts of contrast agents over time in perfusate, bile and liver is illustrated in Fig. 1B (13,21). Each compartment describes the amount of contrast agent over time. Compartment 1 reflects the mixing between KHB and contrast agent solutions when the solutions of perfusion are changed and accounts for the progressive changes of concentrations before the final concentrations (200 or 0 μM) are reached. Compartment 2 (C2) describes the amount of contrast agent in the extracellular space and compartments 4 (C4) and 5 (C5) the amounts in hepatocytes from two distinct compartments. Indeed, the model distinguishes two compartments of hepatocytes C4 and C5 with different concentrations over time (13,21). The transfer between C4 and C5 is unidirectional. From both compartments, a transfer into compartment 6 (C6 or bile compartment) occurs. Compartment 3 represents the amount of contrast agent in the outflow perfusate leaving the liver. Entry of contrast agent into the system is modeled by a zero-order input rate K_{in} over a time period. In the first-order rate constant k_{ij}, i represents the compartment of origin and j the compartment of convergence. The model was implemented in the MATLAB Software (2010b). It was assumed that the rate constant k_{24} is associated with Oatp-mediated hepatic uptake of ^{153}Gd–BOPTA. k_{46} and k_{56} describe Mrp2-dependent canalicular excretion from both hepatocellular compartments and k_{42} is associated with the efflux of ^{153}Gd–BOPTA from hepatocytes back to sinusoids. Pharmacokinetic modeling of contrast agent transport was compared between *fa*/*fa* and *fa*/+ rats.

Additionally, we conducted mathematical simulations and evaluated how modifications of a single parameter representing ^{153}Gd–BOPTA entry into hepatocytes (k_{24}), efflux back from hepatocytes to the extracellular space (k_{42}), or bile excretion from both hepatocellular compartments (k_{46} and k_{56}) modify the hepatic concentration of ^{153}Gd–BOPTA. These simulations mimic the abnormalities that may be observed in cholestatic hepatocytes.

2.7. Statistics

Parameters are means ± SD. A Mann–Whitney test compared means between *fa*/+ and *fa*/*fa* rats. Two-way ANOVA compared the evolution over time of parameters between the experimental groups.

3. RESULTS

3.1. Characteristics of *fa*/+ and *fa*/*fa* Rats

The *fa*/*fa* rats (8 week old) are overweight and have significantly higher serum triglyceride and cholesterol concentrations than *fa*/+ rats (Table 1). Liver weights were greater in obese rats. During liver perfusion, portal pressure was similar in both groups. Moreover, bile flow was significantly lower in *fa*/*fa* (0.6 ± 0.1 μl min^{-1} g^{-1}) than *fa*/+ (1.3 ± 0.1 μl min^{-1} g^{-1}) rats ($p < 0.008$, data not shown). Histology was normal in *fa*/+ rats but steatosis was present in fatty livers (Fig. 1C).

3.2. Concentrations of ^{153}Gd–BOPTA in Hepatocytes from Normal and Fatty Livers (T0–T75)

During the perfusion with the extracellular contrast agent ^{153}Gd–DTPA (Fig. 2A), the hepatic concentrations rapidly increased to a low steady state (<100 nmol g^{-1}). ^{153}Gd–DTPA was then rapidly washed out from the liver during the subsequent KHB perfusion and, as expected, no ^{153}Gd–DTPA was detected in bile (Fig. 3C). At time 45 min (T45), ^{153}Gd–BOPTA was perfused during 30 min before washing with KHB solution. ^{153}Gd–BOPTA hepatic concentrations were much higher than that of ^{153}Gd–DTPA and maximal at T75 (Fig. 2A).

To assess the concentrations of ^{153}Gd–BOPTA within hepatocytes, we must withdraw the concentrations induced by the extracellular distribution of the contrast agent (see Fig. 3A). We can then measure an initial hepatocellular uptake index (IHUI, nmol min^{-1} g^{-1}) from time 46 min (T46) to T49, a period with minimal ^{153}Gd–BOPTA excretion adequate to measure the entry of ^{153}Gd–BOPTA from sinusoids to hepatocytes (Fig. 3A). The IHUI was significantly decreased in *fa*/*fa* rats (27 ± 5 nmol min^{-1} g^{-1}) in comparison to the control group (48 ± 11 nmol min^{-1} g^{-1}; Fig. 3B, $p = 0.008$). After this initial period, concentrations inside hepatocytes reflect both hepatocyte uptake and exit.

In contrast to the hepatic concentrations of ^{153}Gd–BOPTA shown in Fig. 2A (those obtained by the gamma probe), the accumulation and elimination concentrations in Fig. 3D and E only reflect ^{153}Gd–BOPTA concentrations within hepatocytes. At T75, the maximal concentrations were similar in both

Table 1. Characteristics of *fa*/*fa* and *fa*/+ rats

	fa/+ rats	*fa*/*fa* rats	*p*
Age (weeks)	8.5 ± 0.0	8.8 ± 0.5	0.59
Body weight (g)	247 ± 10	328 ± 15	0.002
Liver weight (g)	9.6 ± 0.6	15.5 ± 2.2	0.002
Portal pressure (mmHg)	7.7 ± 1.8	7.4 ± 0.5	0.54
Serum cholesterol (mmol l^{-1})	1.1 ± 0.1	2.2 ± 0.2	0.001
Serum triglycerides (mmol l^{-1})	0.4 ± 0.1	2.3 ± 0.6	0.002
Serum ALAT (UI l^{-1})	79 ± 10	135 ± 25	0.004

Data are means ± SD.

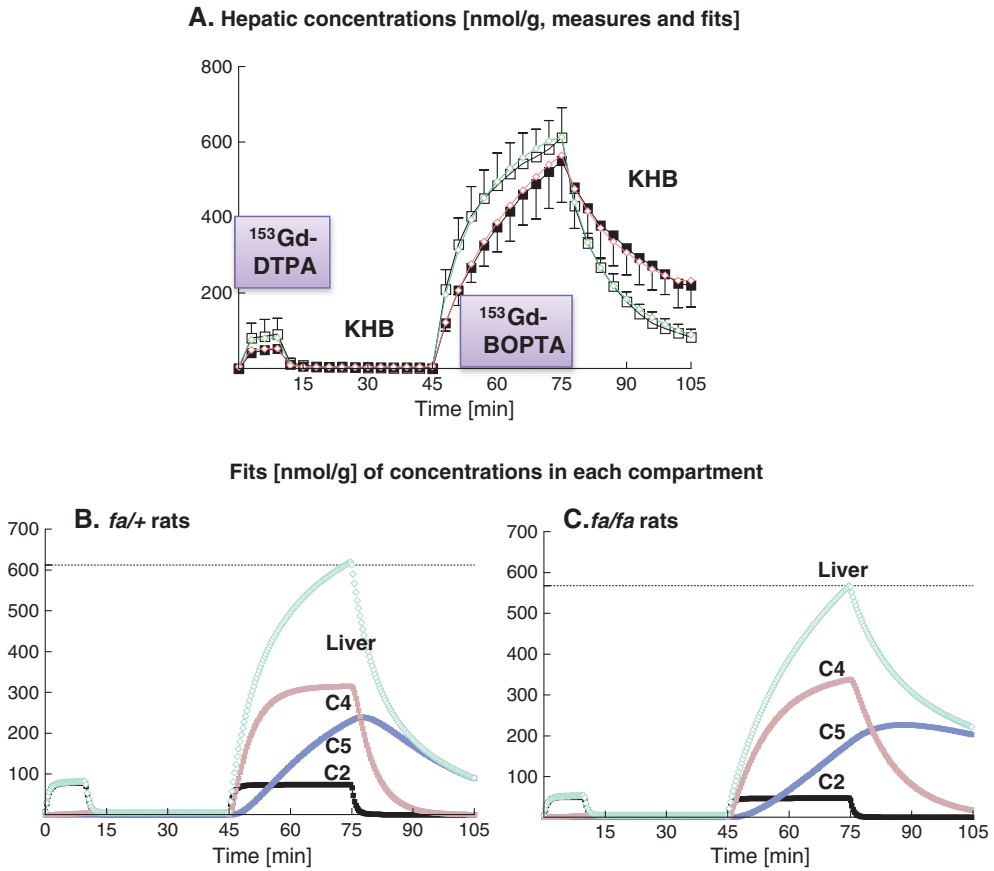

Figure 2. (A) Hepatic concentrations of contrast agents (nmol g^{-1}) during the perfusion of 200 μM ^{153}Gd–DTPA (from 0 to 10 min) and 200 μM ^{153}Gd–BOPTA (from 45 to 75 min). Livers were isolated and perfused from *fa*/+ rats (□ and green fit, $n = 5$) and *fa*/*fa* rats (■ and red fit, $n = 5$). Fits obtained by pharmacokinetic modeling are shown on experimental data. (B and C) Fits of concentrations in each compartment of the liver and in the entire liver from control *fa*/+ rats (B) and *fa*/*fa* rats (C). Liver: total hepatic concentration; C2: extracellular compartment; C4 and C5: hepatocellular compartments.

experimental groups and a two-way ANOVA over time between both groups found no interaction (Fig. 3D, $p = 1.00$). At T75, ^{153}Gd–BOPTA bile accumulation was lower in *fa*/*fa* rats while ^{153}Gd–BOPTA uptake was impossible to measure at this time-point, accumulation reflecting the combination of entry and exit.

3.3. ^{153}Gd–BOPTA Elimination from Hepatocytes (T75–T105)

When ^{153}Gd–BOPTA perfusion was replaced by a KHB solution, ^{153}Gd–BOPTA concentrations within hepatocytes gradually decreased (Fig. 3E). In the absence of ^{153}Gd–BOPTA uptake, the elimination from hepatocytes can be measured by an initial hepatocellular elimination index (IHEI, nmol min^{-1} g^{-1}; Fig. 3E). The IHEI was measured from T76 to T79 and was significantly decreased in *fa*/*fa* rats (-19 ± 5 nmol min^{-1} g^{-1}) vs *fa*/+ rats (-40 ± 12 nmol min^{-1} g^{-1}, $p < 0.008$). Moreover, a two-way ANOVA of concentrations over time between both groups found a positive interaction ($p = 0.05$), the hepatic elimination of ^{153}Gd–BOPTA in *fa*/*fa* rats being significantly lower over time. Interestingly, from T95 to T105, we were able to detect the efflux from hepatocytes back to sinusoids (Fig. 3E). During this period, livers had already been perfused with a KHB solution for 20 min (total volume perfusion: 600 ml into rat livers < 16 g) and we can be sure that the radioactivity measured in outflow perfusate during these last 10 min corresponds to the efflux back of ^{153}Gd–BOPTA from hepatocytes to sinusoids: 64 ± 39 nmol in *fa*/+ rats and 381 ± 105 nmol in *fa*/*fa* rats ($p < 0.008$). During the same period, the bile excretion was 337 ± 69 nmol in *fa*/+ rats and 490 ± 115 nmol in *fa*/*fa* rats ($p = 0.06$). The higher amounts of ^{153}Gd–BOPTA in perfusate and bile of fatty livers despite a decreased transport functions and/or protein expression are explained by increased residual concentrations within hepatocytes (see Discussion) (17–19). At T105, the residual hepatic ^{153}Gd–BOPTA concentrations were 214 ± 60 nmol g^{-1} (*fa*/*fa* rats) and 75 ± 21 nmol g^{-1} (*fa*/+ rats $p < 0.008$). In *fa*/+ rats, 13% of ^{153}Gd–BOPTA elimination was directed to the sinusoids while 44% of ^{153}Gd–BOPTA left hepatocytes through the sinusoidal membrane in *fa*/*fa* rats.

3.4. Pharmacokinetic Modeling of ^{153}Gd–BOPTA Transport in Perfused Rat Livers

To better understand the transport of ^{153}Gd–BOPTA in cholestatic hepatocytes, we performed pharmacokinetic modeling of ^{153}Gd–DTPA and ^{153}Gd–BOPTA transport over time using the compartmental model illustrated in Fig. 1B and described in previous publications (20,21). The model successfully fits the experimental data for both *fa*/*fa* and *fa*/+ rats (Fig. 2A) with three compartments in the liver: an extracellular compartment (C2, depicted by ^{153}Gd–DTPA) and two hepatocellular compartments (C4 and C5). ^{153}Gd–BOPTA from C2 can enter into C4 but not into C5, ^{153}Gd–BOPTA in C5 being provided by C4 without possible return from C5 to C4.

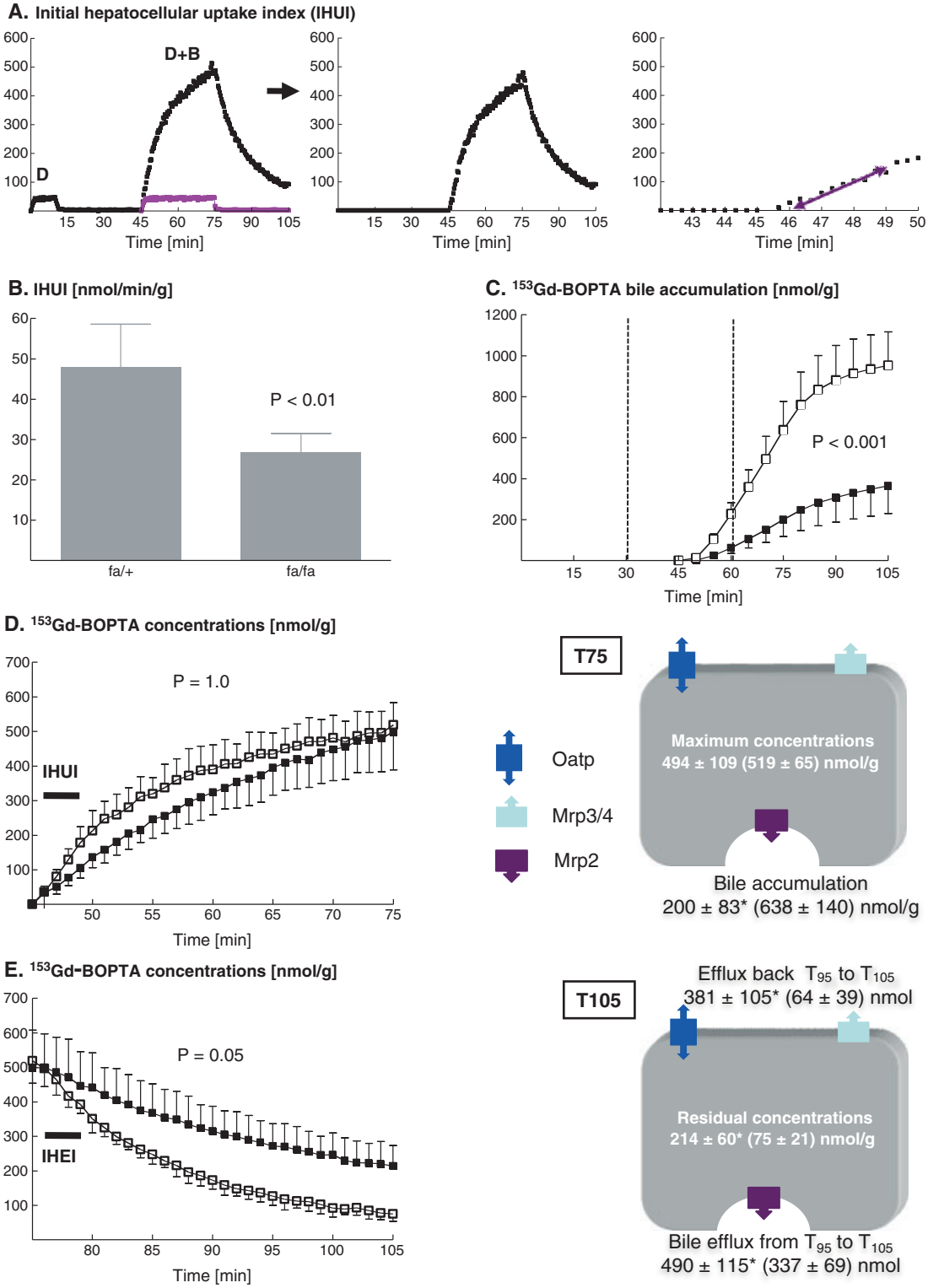

Figure 3. ^{153}Gd–BOPTA concentrations within hepatocytes rely on uptake and exit functions. (A) Uptake is measured by the initial hepatocellular uptake index (IHUI in nmol min^{-1} g^{-1}). For illustration, the concentrations of ^{153}Gd–DTPA (D) and ^{153}Gd–BOPTA (B) in a single liver are shown. The extracellular distribution of ^{153}Gd–DTPA being similar to that of ^{153}Gd–BOPTA, we can obtain the exact ^{153}Gd–BOPTA concentrations over time within hepatocytes. Because few contrast agents are excreted into bile 5 min after the start of the perfusion, the initial slope from time 46 min (T46) to T49 measures the IHUI. B. The IHUI is shown in both experimental groups: control *fa*/+ and fatty *fa*/*fa* rats. (C) ^{153}Gd–BOPTA bile accumulation (nmol g^{-1}) in *fa*/+ (□) and *fa*/*fa* (■) rats. ^{153}Gd–BOPTA accumulation (D) in hepatocytes from T45 to T75 and ^{153}Gd–BOPTA elimination from hepatocytes (E) in *fa*/+ (□) and *fa*/*fa* (■) rats. At T75, the maximal concentrations within hepatocytes and bile excretion are shown. At T105, the residual concentrations within hepatocytes are shown. Efflux back (in nmol) from hepatocytes to sinusoids is compared to bile excretion (nmol) from T95 to T105. Results from *fa*/+ rats are between brackets. Uptake transporters are organic anion transporting polypeptides (Oatps) and exit transporters to bile are multiple resistance-associated proteins 2 (Mrp2). Transporters that return ^{153}Gd-BOPTA back to sinusoids are either Mrp3/4 or Oatps. * $p < 0.05$.

The concentrations of ^{153}Gd–BOPTA in C2 were lower in *fa/fa* than *fa/+* rats (Fig. 2A–C). Because the same concentration of Gd–BOPTA was perfused in both groups, only a larger extracellular distribution volume can explain the decreased hepatic concentrations measured by the gamma probe. In *fa/+* rats, the accumulation in C4 rapidly increased until a plateau is reached by T60 (Fig. 2B). When ^{153}Gd–BOPTA solution was switched to a KHB solution, ^{153}Gd–BOPTA was rapidly eliminated from C4. In C5, ^{153}Gd–BOPTA had a linear accumulation and its maximal accumulation remained lower than that observed in C4. Moreover, the concentrations in C5 remained high during the rinse period with KHB.

The evolution of ^{153}Gd–BOPTA concentrations was different in *fa/fa* rats (Fig. 2C). In fatty livers, the accumulation in C4 was more gradual and, from T75, the elimination was slower than in *fa/+* rats. At T105, the concentrations in C5 were high and corresponded to the increased residual hepatic concentrations.

From the model, rate constants were calculated (Table 2). The hepatic uptake of ^{153}Gd–BOPTA through Oatps (k_{24}) was lower in *fa/fa* rats without reaching statistical significance. The bile excretions from C4 (k_{46}) and C5 (k_{56}) were significantly lower in *fa/fa* rats. Exchange from C4 to C5 (k_{45}) was unidirectional and low in both groups. Efflux from hepatocytes back to sinusoids (k_{42}) was also significantly decreased in fatty livers.

3.5. Pharmacokinetic Modeling and Mathematical Simulations

To understand why the maximal hepatic concentration (at T75) was similar in *fa/fa* and *fa/+* rats, we performed mathematical simulations decreasing a single parameter k_{24} (entry into hepatocytes), k_{46} (bile excretion from C4), k_{56} (bile excretion from C5) or k_{42} (efflux from C4 to sinusoids), while the three others remained unchanged (Fig. 4). With these simulations, we understand how changing a single parameter interferes with hepatic concentrations. Each parameter was modified from the value obtained in *fa/+* rats to 0 (10% change at each step). The values calculated in *fa/fa* livers were found between these extreme values. We showed that, by decreasing k_{24}, the maximal hepatic concentration at T75 decreased until the extracellular ^{153}Gd–BOPTA concentration was reached for $k_{24} = 0$. When k_{46}, k_{56}, or k_{42} were decreased, the maximal hepatic accumulation at T75 increased, and the increase was high with k_{42} set to 0, emphasizing the importance of efflux from hepatocytes to control the intracellular concentrations of ^{153}Gd–BOPTA.

To better understand the hepatic residual concentration, we also performed simulations at T105. The residual hepatic accumulation of ^{153}Gd–BOPTA was moderately modified by the decrease in k_{46} and k_{42} but decreasing k_{56} greatly increased the residual concentration, C5 being the only hepatocellular compartment to retain ^{153}Gd–BOPTA at the end of the protocol.

Finally, to understand the repartition of the contrast agent concentrations in C2, C4, and C5 over time in cholestatic livers, we modified each parameter while the three other parameters remain similar to that calculated in *fa/+* rats (Fig. 5). When k_{24} was set at 0.768 (value close to that of *fa/fa* rats), while k_{46}, k_{56}, and k_{42} remained similar to *fa/+* rats, the hepatic concentration decreased. Modifications of k_{46}, k_{56} or k_{42} increased the hepatic concentration. Interestingly, setting k_{56} at 0.013 increased ^{153}Gd–BOPTA concentrations in C5 over those observed in C4.

4. DISCUSSION

4.1. Relevance of Gd–BOPTA Concentrations within Hepatocytes

The transport of the organic anion Gd–BOPTA across hepatocytes relies on the expression and function of proteins located on the sinusoidal and canalicular membranes. It is relatively easy to measure a single transport parameter in *in vivo* or *in vitro* experimental studies but it is less frequent to measure simultaneously all the parameters (hepatocyte uptake, bile excretion, efflux back to perfusate) as well as the consequences of all parameters on the intracellular concentrations. The hepatic concentrations of Gd–BOPTA depend on the balance between uptake via sinusoidal transporters, biliary excretion and efflux back to sinusoids (either through bidirectional sinusoidal transporters or through sinusoidal Mrp transporters; Fig. 3).

In the experimental model of isolated perfused livers, we evaluate the extracellular space (C2) by measuring Gd–DTPA concentrations. The exact concentrations of Gd–BOPTA within hepatocytes are available (C4 and C5) and the IHUI measures the initial uptake function before the start of bile excretion. Bile excretion of Gd–BOPTA is available during the entire protocol while the efflux back from hepatocytes to sinusoids is evidenced at the end of the study (Fig. 3). During the protocol, the hepatic perfusate flow is constant in all experiments and set to 30 ml min^{-1}, thus the decreased IHUI of fatty livers is not related to changes of hepatic perfusion. In our experimental model, liver isolation precludes interferences with extrahepatic organs. The composition of solutions is well controlled and does not include binding

Table 2. Hepatic pharmacokinetics by compartmental analysis

Rate constants (min^{-1})	*fa/+* rats	*fa/fa* rats	*p*
k_{12}	1.19 ± 0.13	1.33 ± 0.36	0.42
k_{23}	9.60 ± 4.52	9.27 ± 1.44	1.00
k_{24}	0.96 ± 0.39	0.79 ± 0.17	0.55
k_{42}	0.11 ± 0.02	0.05 ± 0.01	0.008
k_{45}	0.05 ± 0.02	0.03 ± 0.01	0.10
k_{46}	0.065 ± 0.011	0.025 ± 0.007	0.008
k_{56}	0.045 ± 0.008	0.013 ± 0.006	0.008

The rate constant k_{24} is associated with ^{153}Gd-BOPTA uptake. k_{46} and k_{56} describe bile excretion in C6 from the hepatic compartments C4 and C5. k_{42} is associated with the efflux of ^{153}Gd-BOPTA from hepatocytes back to sinusoids.

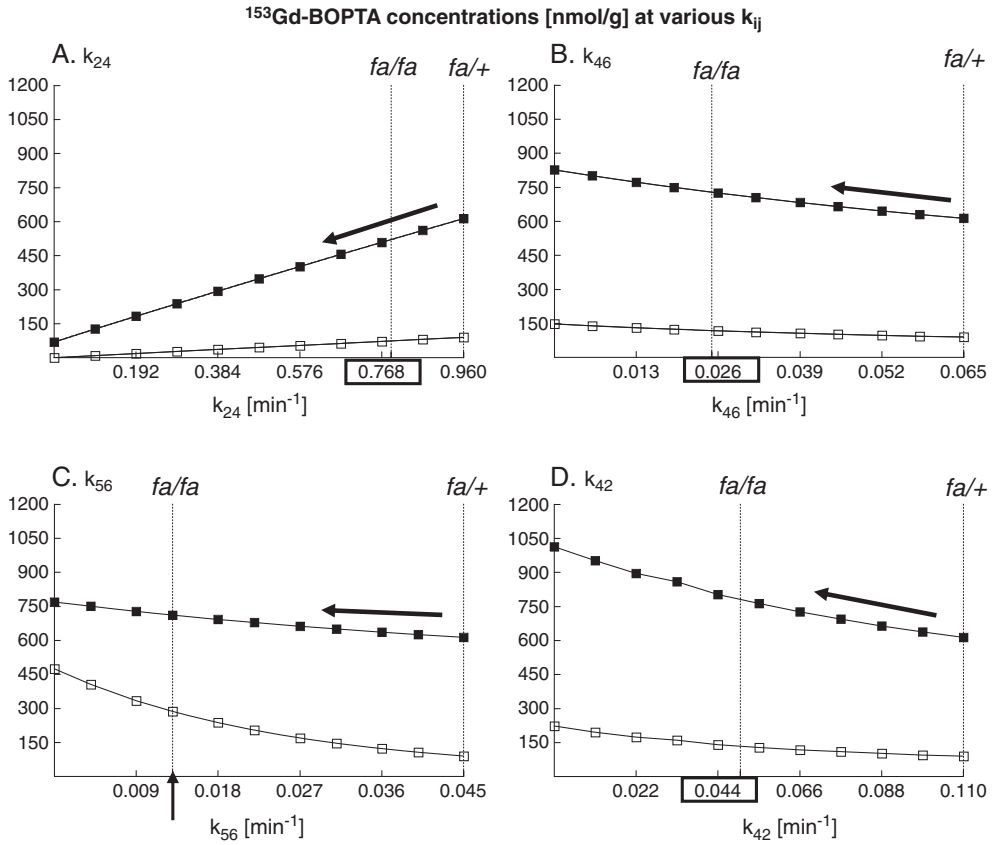

Figure 4. Mathematical simulations of ^{153}Gd–BOPTA concentrations (nmol g^{-1}) at various k_{ij} according to the pharmacokinetic model presented in Fig. 1B A single parameter representing ^{153}Gd–BOPTA entry into hepatocytes (A, k_{24}), bile excretion from both hepatocellular compartments (B, k_{46} and C, k_{56}), and efflux back from hepatocytes to the extracellular space (D, k_{42}), was modified from the value obtained in control *fa*/+ rats to 0 (10% change at each step on the *x*-axis). The consequences of changing a single parameter on ^{153}Gd–BOPTA hepatic concentrations (nmol g^{-1}) were calculated. Hepatic accumulations were calculated at T75 (■) and T105 (□). Decreasing k_{24} (^{153}Gd–BOPTA uptake into hepatocytes) lowers hepatic concentrations. Decreasing k_{42} (efflux through the sinusoidal membrane), k_{46} or k_{56} (efflux through the canalicular membrane) augments them.

proteins. Because the transport of Gd–BOPTA through transporters is related to the concentration gradients of the contrast agent between sinusoids, hepatocytes and bile, we administered Gd–BOPTA at steady concentrations rather than as a bolus injection similarly to the clinical situation.

Understanding the function of transporters is important to evidence how Gd–BOPTA accumulates in hepatocytes. Cholestatic fatty livers from *fa/fa* rats have a decreased expression of Oatp1a4 (17,18) and Mrp2 (17,19). Interestingly, Mrp3 and Mrp4 are increased in another experimental model of fatty livers (6). In addition to the expression of transporters, other function regulations were described. Phosphorylation of Mrp2 can retrieve the transporter from the canalicular membrane and trap Gd–BOPTA within rat hepatocytes (14,22,23). Entry of Gd–BOPTA into hepatocytes is also impaired by drug–drug interaction when Gd–BOPTA is perfused together with bromosulfophthalein (24).

Thus, it is important to assess the function of transporters in injured hepatocytes. We show that fatty hepatocytes have a decreased uptake function as measured by the decreased uptake index (IHUI). The elimination function of Gd–BOPTA from hepatocytes is also impaired, as shown by the decrease in the IHEI, $k_{46,}$ and k_{56}. Gd–BOPTA may also exit from hepatocytes by efflux back to sinusoids and this function is also impaired in fatty livers (decreased k_{42}). However, the amounts of Gd–BOPTA that exit from hepatocytes during the period T95–T105 are higher in fatty than control livers because the residual concentrations are higher during this period. The amounts (*A*) of Gd–BOPTA transported through the sinusoidal membrane back to hepatic vessels are defined by the equation: A (nmol min^{-1} g^{-1}) = k_{42} (min^{-1}) × C (nmol g^{-1}), where C is the concentration in hepatocytes. Thus, Gd–BOPTA amount transported back to sinusoids in fatty hepatocytes can be higher that in normal hepatocytes even though the transport function through Oatps is decreased. We previously showed, that the efflux back to sinusoids and bile excretion in normal hepatocytes are proportional to the concentrations inside livers (13). This point emphasizes the importance of concentrations within hepatocytes in the regulation of transport proteins. Of note, we do not distinguish the mechanisms that induce a decreased transport of Gd–BOPTA through membrane proteins in fatty hepatocytes: either decreased expression of transporters and/or dysregulation of protein function.

4.2. Hepatobiliary Contrast Agents and Liver Imaging

The clinical importance of our findings is provided by recent studies that investigated the hepatic accumulation of Gd–BOPTA and the other closely related compound Gd–EOB–DTPA (Primovist®, Bayer, Germany). In multinodular focal fatty infiltrations, Marin *et al.* (10) found a decreased signal intensities during the vascular and equilibrium phases following the injection of Gd–BOPTA, a finding similar to the decreased concentrations of the contrast agent in C2 from *fa/fa* livers. However, in contrast to our results,

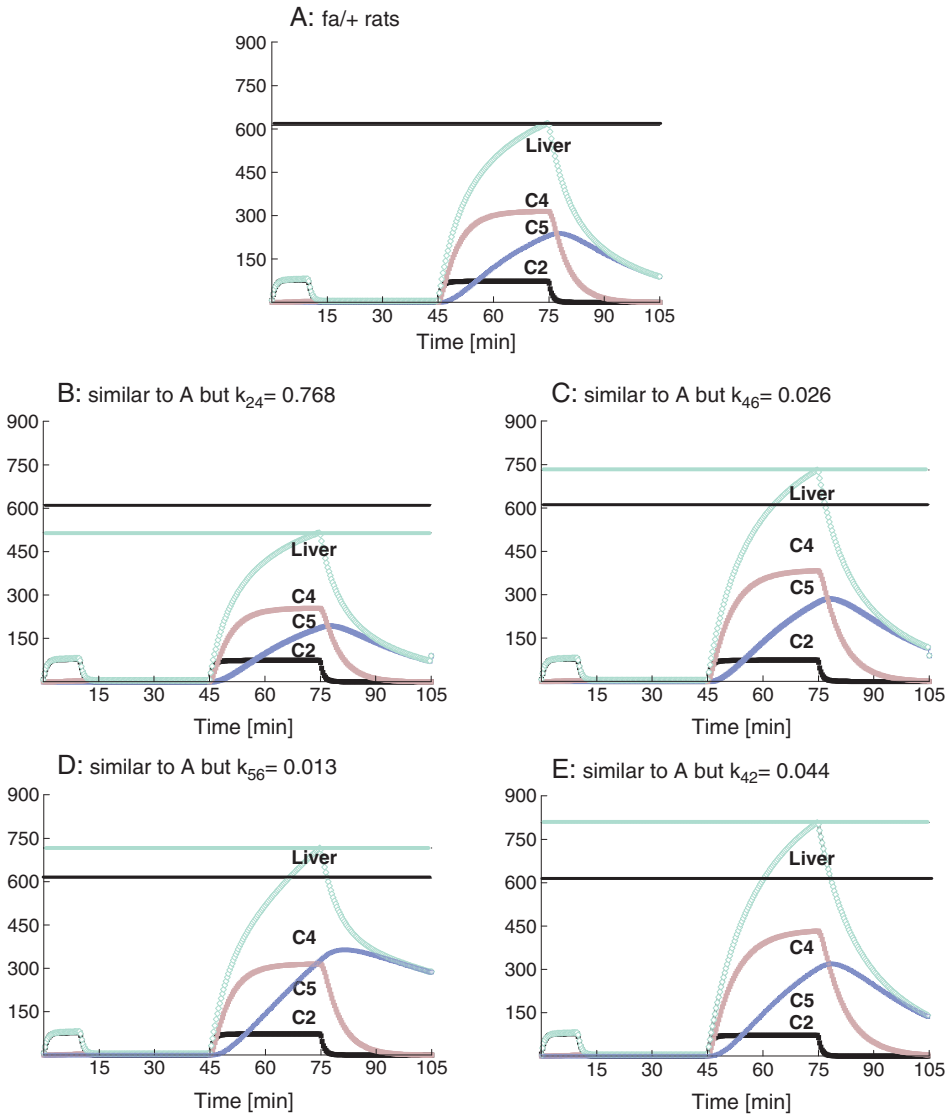

Figure 5. Concentrations of ^{153}Gd–DTPA and ^{153}Gd–BOPTA (nmol g^{-1}): effect of changing a single parameter. The pharmacokinetics over time of ^{153}Gd–BOPTA concentrations in *fa*/+ rats is shown in the entire liver (green), compartment 2 (C2 or extracellular compartment, black), C4 (hepatocytes, brown), and C5 (hepatocytes, purple) (A). Pharmacokinetics was calculated in *fa*/+ rats with k_{24} set to 0.768 (B), *fa*/+ rats with k_{46} = 0.026 (C), *fa*/+ rats with k_{24} = 0.013 (D), and *fa*/+ rats with k_{42} = 0.044 (E). These figures illustrate how changing a single k_{ij} (from the value measured in *fa*/+ rats to that measured in *fa*/*fa* rats) modifies the distribution of ^{153}Gd–BOPTA in the entire liver, C3, and C4. The black horizontal line shows the maximal concentration obtained in *fa*/+ livers and the green horizontal one, the maximal concentration obtained with a single k_{ij} change.

Gd–BOPTA did not enter human fatty hepatocytes and the lesions were hypointense in comparison to surrounding normal parenchyma. In rats with nonalcoholic steatohepatitis, the maximal intensity following a bolus of Gd–EOB–DTPA was similar to normal rats while the elimination was delayed (25). In this experimental model, the expression of Oatps and Mrp2 was similar in normal and fatty livers. However, the function of the transporters could not be determined.

4.3. Pharmacokinetic Modeling of Gd–BOPTA Transport

In previous studies, we described the pharmacokinetics of Gd–DTPA and Gd–BOPTA transport by compartmental analysis in normal rats (21,26). Such modeling is a valuable tool to understand the kinetic of drug concentrations in various compartments over time. The best model includes six compartments and eight rate constants. We show that this model perfectly fits the experimental data in both normal and fatty livers. The extracellular distribution volume is higher in fatty liver, and the evolution of Gd–BOPTA accumulation is different in both hepatocellular compartments C4 and C5. In C4 of normal livers, the initial accumulation rate is high until a plateau is reached. Gd–BOPTA is rapidly excreted from this compartment during the rinse period. Accumulation in C5 is more linear and late to disappear. In fatty livers, the accumulation in C4 is more gradual without reaching a plateau and the emptying is slower. Chandra *et al.* (27) also found two hepatocellular compartments in isolated rat livers perfused with 5-(and 6)-carboxy-2′,7′ dichlorofluorescein, which uses the same Oatps/Mrp2 pathway as Gd–BOPTA. The signification of two cellular compartments is puzzling but we can speculate that Gd–BOPTA accumulation in C4 is close to the canalicular membrane because its hepatic elimination is rapid.

4.4. Mathematical Simulations

Pharmacokinetic modeling with mathematical simulations has already been performed to better understand the hepatobiliary transport of drugs through the Oatps/Mrp2 pathway. Thus, in healthy volunteers, a pharmacokinetic model was developed based on blood, urine, and bile concentration-time profiles after the injection of ^{99m}Tc-mebrofenin (28). In this model, mathematical simulations were also performed to evaluate how decreasing the transport through OATPs, MRP2, or both OATPs and MRP2, would influence the hepatic accumulation (28). Interestingly, liver imaging with ^{99m}Tc-mebrofenin also represents the accumulation of tracers (29,30).

Our simulations show that hepatic concentrations over time are the result of four biological processes: hepatocyte uptake through Oatps (k_{24}), bile excretion through Mrp2 (two parameters: k_{46} and k_{56}) and efflux back to sinusoids (k_{42}). The most important parameters are those located on the sinusoidal membrane, a finding in line with the evidence that a compound that does not enter into hepatocytes will not be excreted in bile. Finally, to understand the repartition of the contrast agent over time in C2, C4 and C5 in cholestatic livers, we modified each parameter while the three other parameters remain similar to that calculated in normal livers rats. When k_{24} was set at 0.768 (value close to that of fatty livers), while k_{46}, k_{56} and k_{42} remained similar to normal livers, the hepatic accumulation decreased. Decreasing k_{46}, k_{56} or k_{42} increased the hepatic accumulation.

In summary, we show that cholestatic hepatocytes have similar maximal concentrations of Gd–BOPTA than normal cells despite a decreased function of Oatps and Mrp2. The study emphasizes the importance of concentrations of organic anions within hepatocytes for the transport function through membrane proteins. Although complex, such understanding is important to analyze liver imaging with hepatobiliary contrast agents in cholestatic fatty livers. Moreover, we describe an index of hepatocellular uptake function (IHUI) that may score the severity of fatty livers in clinical liver MRI associated with the injection of hepatobiliary contrast agents.

Acknowledgement

This work was supported by the Fonds National Suisse de la Recherche Scientifique to C.M. Pastor (grant 310030-126030).

REFERENCES

1. Fabbrini E, Sullivan S, Klein S. Obesity and nonalcoholic fatty liver disease: biochemical, metabolic, and clinical implications. Hepatology 2010; 51: 679–689.
2. Arrese M, Trauner M. Molecular aspects of bile formation and cholestasis. Trends Mol Med 2003; 9: 558–564.
3. Arrese M, Karpen SJ. Nuclear receptors, inflammation, and liver disease: insights for cholestatic and fatty liver diseases. Clin Pharmacol Ther 2010; 87: 473–478.
4. Wagner M, Zollner G, Trauner M. New molecular insights into the mechanisms of cholestasis. J Hepatol 2009; 51: 565–580.
5. Zollner G, Wagner M, Trauner M. Nuclear receptors as drug targets in cholestasis and drug-induced hepatotoxicity. Pharmacol Ther 2010; 126: 228–243.
6. Lickteig AJ, Fisher CD, Augustine LM, Aleksunes LM, Besselsen DG, Slitt AL, Manautou JE, Cherrington NJ. Efflux transporter expression and acetaminophen metabolite excretion are altered in rodent models of nonalcoholic fatty liver disease. Drug Metab Dispos 2007; 35: 1970–1978.
7. Ma X, Holalkere NS, Kambadakone RA, Mino-Kenudson M, Hahn PF, Sahani DV. Imaging-based quantification of hepatic fat: methods and clinical applications. Radiographics 2009; 29: 1253–1277.
8. Reeder SB, Cruite I, Hamilton G, Sirlin CB. Quantitative assessment of liver fat with magnetic resonance imaging and spectroscopy. J Magn Reson Imag 2011; 34: 729–749.
9. Springer F, Machann J, Claussen CD, Schick F, Schwenzer NF. Liver fat content determined by magnetic resonance imaging and spectroscopy. World J Gastroenterol 2010; 16: 1560–1566.
10. Marin D, Iannaccone R, Catalano C, Passariello R. Multinodular focal fatty infiltration of the liver: atypical imaging findings on delayed T1-weighted Gd-BOPTA-enhanced liver-specific MR images. J Magn Reson Imag 2006; 24: 690–694.
11. Tsuda N, Okada M, Murakami T. New proposal for the staging of nonalcoholic steatohepatitis: evaluation of liver fibrosis on Gd-EOB-DTPA-enhanced MRI. Eur J Radiol 2010; 73: 137–142.
12. Yamamoto A, Tamada T, Sone T, Higashi H, Yamashita T, Ito K. Gd-EOB-DTPA-enhanced magnetic resonance imaging findings of nondiffuse fatty change of the liver. J Comput Assist Tomogr 2010; 34: 868–873.
13. Millet P, Moulin M, Stieger B, Daali Y, Pastor CM. How organic anions accumulate in hepatocytes lacking Mrp2: evidence in rat liver. J Pharmacol Exp Ther 2011; 336: 624–632.
14. Planchamp C, Hadengue A, Stieger B, Bourquin J, Vonlaufen A, Frossard J-L, Quadri R, Becker CD, Pastor CM. Function of both sinusoidal and canalicular transporters controls the concentration of organic anions within hepatocytes. Mol Pharmacol 2007; 71: 1089–1097.
15. de Haën C, Lorusso V, Tirone P. Hepatic transport of gadobenate dimeglumine in TR- rats. Acad Radiol 1996; 3: S452–S454.
16. Planchamp C, Montet X, Frossard J-L, Quadri R, Stieger B, Meier PJ, Ivancevic MK, Vallée J-P, Terrier F, Pastor CM. Magnetic resonance imaging with hepatospecific contrast agents in cirrhotic rat livers. Invest Radiol 2005; 40: 187–194.
17. Geier A, Dietrich CG, Grote T, Beuers U, Prüfer T, Fraunberger P, Matern S, Gartung C, Gerbes AL, Bilzer M. Characterization of organic anion transporter regulation, glutathione metabolism and bile formation in the obese Zucker rat. J Hepatol 2005; 43: 1021–1030
18. Kim MS, Wang S, Shen Z, Kochansky CJ, Strauss JR, Franklin RB, Vincent SH. Differences in the pharmacokinetics of peroxisome proliferator-activated receptor agonists in genetically obese Zucker and Sprague-Dawley rats: implications of decreased glucuronidation in obese Zucker rats. Drug Metab Dispos 2004; 32: 909–914.
19. Pizarro M, Balasubramaniyan N, Solís N, Solar A, Duarte I, Miquel JF, Suchy FJ, Trauner M, Accatino L, Ananthanarayanan M, Arrese M. Bile secretory function in the obese Zucker rat: evidence of cholestasis and altered canalicular transport function. Gut 2004; 53: 1837–1843.
20. Planchamp C, Gex-Fabry M, Becker CD, Pastor CM. Model-based analysis of Gd-BOPTA-induced MR signal intensity changes in cirrhotic rat livers. Invest Radiol 2007; 42: 513–521.
21. Planchamp C, Pastor CM, Balant L, Becker CD, Terrier F, Gex-Fabry M. Quantification of Gd-BOPTA uptake and biliary excretion from dynamic MRI in rat livers: model validation with ^{153}Gd-BOPTA. Invest Radiol 2005; 40: 705–714.
22. Dombrowski F, Kubitz R, Chittattu A, Wettstein M, Saha N, Haussinger D. Electron-microscopic demonstration of multidrug resistance protein 2 (Mrp2) retrieval from the canalicular membrane in response to hyperosmolarity and lipopolysaccharide. Biochem J 2000; 348: 183–188.
23. Beuers U, Bilzer M, Chittattu A, Kullak-Ublick GA, Keppler D, Paumgartner G, Dombrowski F. Tauroursodeoxycholic acid inserts the apical conjugate export pump, Mrp2, into canalicular membranes and stimulates organic anion secretion by protein kinase C–dependent mechanisms in cholestatic rat liver. Hepatology 2001; 33: 1206–1216.
24. Pastor CM, Planchamp C, Pochon S, Lorusso V, Montet X, Mayer J, Terrier F, Vallée J-P. Kinetics of gadobenate dimeglumine in isolated perfused rat liver: MR imaging evaluation. Radiology 2003; 229: 119–125.
25. Tsuda N, Matsui O. Signal profile on Gd-EOB-DTPA-enhanced MR imaging in non-alcoholic steatohepatitis and liver cirrhosis induced in rats: correlation with transporter expression. Eur Radiol 2011; 21: 2542–2550.
26. Planchamp C, Beyer GJ, Slosman DO, F Terrier F, Pastor CM. Direct evidence of the temperature dependence of Gd-BOPTA transport in the intact liver. Appl Radiat Isot 2005; 62: 943–949.

27. Chandra P, Johnson BM, Zhang P, Pollack GM, Brouwer KL. Modulation of hepatic canalicular or basolateral transport proteins alters hepatobiliary disposition of a model organic anion in the isolated perfused rat liver. Drug Metab Dispos 2005; 33: 1238–1243.
28. Ghibellini G, Leslie EM, Pollack GM, Brouwer KL. Use of Tc-99 m mebrofenin as a clinical probe to assess altered hepatobiliary transport: integration of in vitro, pharmacokinetic modeling, and simulation studies. Pharm Res 2008; 25: 1851–1860.
29. Bhargava KK, Joseph B, Ananthanarayanan M, Balasubramaniyan N, Tronco GG, Palestro CJ, Gupta S. Adenosine triphosphate-binding cassette subfamily C member 2 is the major transporter of the hepatobiliary imaging agent (99 m)Tc-mebrofenin. J Nucl Med 2009; 50: 1140–1146.
30. de Graaf W, Bennink RJ, Heger M, Maas A, de Bruin K, van Gulik TM. Quantitative assessment of hepatic function during liver regeneration in a standardized rat model. J Nucl Med 2011; 52: 294–302.